High-Pressure- and Low-Temperature-Induced Changes in $[(CH_3)_2NH(CH_2)_2NH_3][SbCl_5]$

Maciej Bujak* and Ross J. Angel

Crystallography Laboratory, Department of Geosciences, Virginia Tech, Blacksburg, Virginia 24061

Received: January 31, 2006; In Final Form: April 11, 2006

The structure of *N*,*N*-dimethylethylenediammonium pentachloroantimonate(III), $[(CH_3)_2NH(CH_2)_2NH_3][SbCl_5]$, NNDP, was investigated at 100 and 15 K at ambient pressure, as well as at pressures up to 4.00 GPa at room temperature in the diamond-anvil cell. The stable structure at low temperatures and low pressures consists of isolated $[SbCl_5]^{2-}$ anions and $[(CH_3)_2NH(CH_2)_2NH_3]^{2+}$ cations. The inorganic anions have a distorted square pyramidal geometry. They are arranged in linear chains parallel to the *c* axis. In contrast to the low-temperature studies, where no phase transition was detected, pressure induces a $P2_1/c \rightarrow P2_1/n$ phase transition between 0.55 and 1.00 GPa, accompanied by a doubling of the *a* unit-cell parameter. This solid−solid transition results from changes in the electron configuration of the Sb^{III} atom and formation of the Sb−Cl bridging bonds between inorganic polyhedra to form, at ∼1.0 GPa, isolated $[Sb_2Cl_{10}]^{4-}$ units consisting of $[SbCl_6]^{3-}$ octahedra and $[SbCl_5]^{2-}$ square pyramids connected by a common corner. The intermolecular distances continuously decrease with further increase in pressure, and at ∼3.1 GPa, zigzag $[\{SbCl_5\}_n]^{2n-}$ chains containing corner-sharing $[SbCl_6]^{3-}$ octahedra are formed. The unit-cell volume of NNDP decreases by 18.15% between room pressure and 4.00 GPa. The linear distortions of the $[SbCl_5]^{2-}$ and $[SbCl_6]^{3-}$ polyhedra decrease with increasing pressure and decreasing temperature and indicate a reduction in the stereochemical activity of the lone electron pair on the Sb^{III} atom.

1. Introduction

The interest in chloroantimonates(III) with organic cations derives from two main facts. First, the crystals undergo phase transitions, some of them to polar phases, which arise from the large polarizability of the complex anions, changes in the dynamic disorder of the organic cations, and consequent changes in the hydrogen-bonding scheme. Second, the inorganic chloroantimonate(III) anions may assume several structural geometries with varying degrees of distortion depending on the size, symmetry, and ability to form hydrogen bonds to the organic cations.[1−3] Moreover, because chloroantimonates(III) display a wide range of interactions, they offer the unique possibility to compare the relative importance of the stereochemical activity of the lone electron pair on the Sb^{III} atom, N(C)−H···Cl hydrogen bonds, Cl···Cl contacts (dihalogen bonds), and Sb···Cl interactions in understanding the: (i) formation of inorganic polyanions, (ii) distortions of polyhedra, (iii) mechanisms of phase transitions, and (iv) generations of polar ferroelectric or pyroelectric properties in hybrid organic−inorganic materials.

Because of the "secondary bonding" effects, intermolecular hypervalent interactions, i.e., contacts in the range between a bond and a van der Waals interaction, the bond lengths and angles in structures of chloroantimonates(III) are known to deviate from regularity.[4−7] This behavior has been described and rationalized, among others, by Gillespie in terms of the valence shell electron pair repulsion (VSEPR) model.[8,9] In a series of our recent papers, we have correlated the differences in Sb−Cl bond lengths to a "primary deformation" connected with the tendency of $[SbCl_6]^{3-}$ octahedra and $[SbCl_5]^{2-}$ square pyramids to share halogen atoms with each other and a "secondary deformation" resulting from the presence of interactions between oppositely charged organic and inorganic components of the structures.[10−12] Owing to these two different phenomena, which are connected with the presence of the lone electron pair on the Sb^{III} central atom,[13−15] the Sb−Cl bond lengths differ from each other within the same polyhedron by as much as ∼1 Å. We have also demonstrated that significant changes in Sb−Cl bond lengths take place with decreasing temperature. The largest changes, of about 0.3 Å, are associated with changes in the hydrogen-bonding scheme across a phase transition.[16,17] Smaller changes, ∼0.05 Å, are associated with either ordering of organic cations or decreasing of donor··· acceptor distances of hydrogen bonds on decreasing temperature.[18−20]

N,*N*-dimethylethylenediammonium pentachloroantimonate(III), $[(CH_3)_2NH(CH_2)_2NH_3][SbCl_5]$, (hereafter referred as NNDP) is useful as a model structure for understanding the various factors influencing distortions of inorganic polyhedra and generation of phase transitions in this class of compounds because the organic cations are fully ordered, and the inorganic component consists of single isolated $[SbCl_5]^{2-}$ units. In NNDP at ambient conditions[12] the $[SbCl_5]^{2-}$ polyhedra have a distorted square pyramidal geometry, with one short axial and four longer equatorial Sb−Cl distances, as a result of the Sb^{III} lone electron pair occupying the sixth corner of the coordination polyhedron around the Sb atom. The $[SbCl_5]^{2-}$ polyhedra are aligned in chains parallel to [001] such that an equatorial Sb−Cl bond of one polyhedron is directed toward the base of a neighboring $[SbCl_5]^{2-}$ polyhedra with a Sb···Cl distance of 3.667(2) Å (Figure 1). The voids between the inorganic polyhedra are filled by $[(CH_3)_2NH(CH_2)_2NH_3]^{2+}$ organic cations. They are hydrogen bonded to $[SbCl_5]^{2-}$ units. The hydrogen-bonding influence is clearly visible in the differences of lengths of the equatorial Sb−Cl bonds (Figure 1).

* Corresponding author. E-mail: mbujak@uni.opole.pl. Telephone/Fax number: + 48 77 4410741. Permanent address: Institute of Chemistry, University of Opole, Oleska 48, 45-052 Opole, Poland.

10.1021/jp060652v CCC: $33.50
Published on Web 05/12/2006

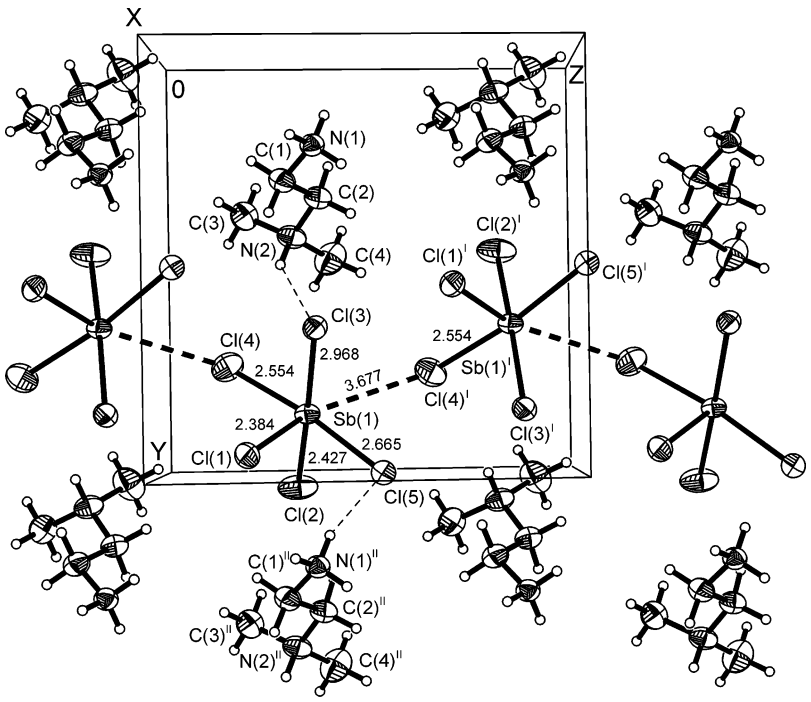

Figure 1. Packing diagram of the NNDP crystal at ambient conditions. The origin of the unit cell has been moved by $[-1/2\ 0\ 0]$ from that reported by Bujak and Zaleski.[12] The thick dashed lines show the closest Sb···Cl interactions. The thin dashed lines depict the N−H···Cl hydrogen bonds. Displacement ellipsoids are drawn at 50% probability level. Symmetry codes: (I) $x, -y + 3/2, z + 1/2$; (II) $x, y + 1, z$.

Changes in the structure of NNDP with temperature or pressure must therefore be due to the intrinsic properties of the inorganic anion and changes in hydrogen-bonding distances and geometry, and not due to effects arising from ordering of the organic cation. NNDP thus provides the possibility of evaluating the role of these mechanisms in the phase transition behavior of other chloroantimonates(III) in which the interactions and phase transition behavior will be more complex as a result of changes in the dynamics of the organic cations. We have therefore undertaken a crystallographic study of the behavior of NNDP both to low temperatures (15 K) and to high pressures in order to determine whether the structural evolution is due solely to the removal of thermal energy as temperature is decreased or whether the reduction of interatomic distances plays a dominant role.

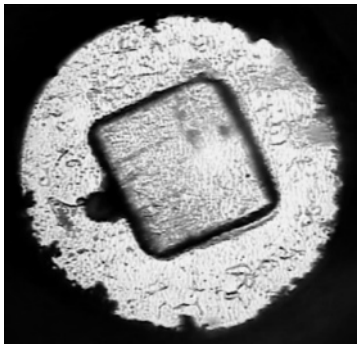

Figure 2. Single crystal of NNDP in the high-pressure ETH diamond-anvil cell at 4.00 GPa. A small ruby ball is visible near the left edge of the crystal. The mottled appearance is, in part, due to small crystals of solidified nitrogen.

2. Experimental Methods

2.1. Preparation of Single Crystals of NNDP. Antimony(III) oxide (puriss. p. a., Fluka), *N*,*N*-dimethylethylenediamine (95%, Sigma-Aldrich), and concentrated hydrochloric acid (36.5−38%, EM Science) were the starting materials used for the synthesis of NNDP. Sb_2O_3 (2.915 g, 10 mmol) dissolved in ca. 25 mL of hot concentrated HCl were treated with 1.15 mL (10 mmol) of *N*,*N*-dimethylethylenediamine dissolved in 4.0 mL of ca. 6 M HCl. Transparent colorless plates suitable for the single-crystal X-ray diffraction studies were grown by slow evaporation of the acid solution at room temperature.

2.2. Crystal Structure Determinations at Low Temperature. Intensity data were collected on an Oxford Diffraction Xcalibur-2 diffractometer equipped with an Enhance X-ray source (graphite monochromated Mo Kα) and a Sapphire-3 CCD detector. The Oxford Diffraction Cryojet XL and Helijet coolers were used for the measurements at 100 and 15 K, respectively. All accessible reflections were measured using the φ- and ω-scan techniques with $\Delta\omega = 1.0°$ and $\Delta t = 25$ and 5 s, respectively. The unit-cell parameters were obtained from a least-squares refinement of 10 671 and 9938 reflections at 100 and 15 K, respectively. The data were subjected to numerical absorption corrections.[21] All hydrogen atoms were located in the subsequent difference electron density maps.

2.3. Crystal Structure Determinations at High Pressure. An NNDP crystal in the form of a (100) plate was loaded and pressurized in an ETH diamond-anvil cell (DAC).[22] The diameter of the diamond culets was 0.84 mm. The gasket, made of 0.25-mm-thick hard T301 steel foil, was pre-indented to a thickness of ca. 0.21 mm, and then a hole of 0.50 mm in diameter was spark-eroded in the center of the indented region. The sample crystal was fixed on the surface of an anvil together with a small ruby ball (ca. 0.02 mm in diameter), using a petroleum jelly previously immersed for a few days in isopropyl alcohol. Because the NNDP crystals dissolve in the alcohols commonly used as pressure media for high-pressure diffraction experiments, e.g., ref 23, cryogenically loaded nitrogen was used as a pressure-transmitting medium (Figures 2 and 3). Previous measurements indicated that the nitrogen remains hydrostatic up to its freezing pressure of 3.0 GPa at room temperature and supports only weak deviatoric stresses at the maximum pressure of 4.00 GPa achieved in these experiments.[24] Pressures, with

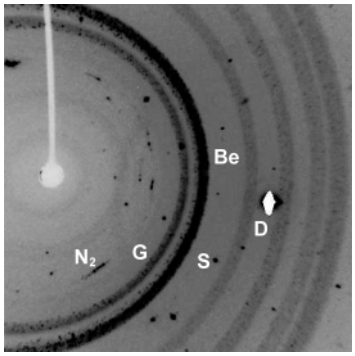

Figure 3. Data collection frame of the NNDP crystal at 4.00 GPa in ETH diamond-anvil cell loaded with nitrogen. Reflections from the sample are labeled "S", those from diamonds "D". The powder diffraction rings derive from the gasket material, beryllium backing disks and solidified nitrogen are labeled "G", "Be", and "N_2", respectively.

an accuracy of ca. 0.05 GPa, were determined from the shift of the ruby *R*-luminescence lines[25] by using a Dilor XY 0.64m Raman microprobe and accessory spectrometer with CCD multichannel detector.

High-pressure intensity data were collected on an Oxford Diffraction Xcalibur-1 diffratometer using monochromated Mo Kα radiation and a Sapphire-2 CCD detector. At each pressure, the single crystal of NNDP was first approximately centered on the diffractometer by optical observation. More precise centering was achieved in an iterative process by using the setting angles of 50−70 strong low-angle reflections to determine the crystal offsets from the center of the goniometer.[26,27] All accessible data were measured by using the ω-scan technique with $\Delta\omega = 1.0°$ and $\Delta t = 100$ s, giving typical total data collection times of 40−42 h per pressure point. The same NNDP single crystal in the same orientation in the same DAC was used for all high-pressure data collections.

The unit-cell parameters were determined at each high-pressure point from a least-squares fit to the corrected setting angles of 20−29 reflections obtained by the eight-position centering method[29] on a Huber four-circle diffractometer, equipped with a Mo Kα sealed-tube source, driven by the Single software.[28] The values of symmetry-constrained unit-cell parameters obtained by vector-least-squares refinement[30] are shown in Table 1.

2.4. Data Reduction. In both the low-temperature and high-pressure studies, the Oxford Diffraction CrysAlis CCD and CrysAlis RED software were used for data collection and data reduction.[21] All data were corrected for Lorentz and polarization effects. In addition, the high-pressure data were corrected for absorption effects of the DAC (i.e., shadowing by the gasket and absorption by the beryllium backing plates and diamond anvils) and the sample.[31,32] The Average v2.2 program, with options to reject outliers from sets of symmetry-equivalent data, including the effects of "diamond dips" in diamond-anvil cell data, was used to average crystallographically equivalent reflections.[33] The remaining independent reflections were used to solve and refine the structures.

SHELXTL NT was used for the structure solutions and refinements,[34] and all structures were solved by the Patterson method. All Sb, Cl, N, and C atoms were refined with anisotropic displacement parameters. For room- and high-pressure structures, all of the hydrogen atoms were refined by using a riding model and constrained to the distances of 0.89, 0.91, 0.96, and 0.97 Å for $-NH_3^+$, $\equiv NH^+$, $-CH_3$, and $=CH_2$ groups, respectively. The occupancies of the hydrogen atoms were set identical to their carriers. Their displacement parameters were taken with coefficients 1.5 and 1.2 times larger than the respective parameters of the methyl C and remaining methylene C and N atoms. The lower-quality data from the diamond-anvil cell meant that it was necessary to use restraints on the anisotropic displacement parameters for non-H atoms and to add hydrogen atoms by using the standard geometric criteria. The structure drawings were prepared by using the XP program within SHELXTL NT.[34]

The crystal data and the structure determination details are listed in Table 1. The bond lengths, angles, and the hydrogen bond geometries are presented in Tables 2, 3, and 4. Because the body of the diamond-anvil cell restricts the range of reflections that are accessible to measurement,[23] the resulting lack of resolution in certain crystallographic directions can lead to a bias in the values of the refined parameters compared to a structure refined to a full dataset collected in air, e.g., ref 35. To prevent such biases affecting our analysis of the structural evolution of NNDP, in the following discussion, we use the previously reported structural parameters for NNDP crystal at ambient conditions[12] as a basis for comparison of the low-temperature data. In the discussion of the high-pressure results, the geometrical parameters determined from the NNDP crystal loaded in the DAC without pressure fluid (the 297 K/0.1 MPa data in Tables 1, 3, and 4) were used.

3. Results and Discussion

The structure of NNDP at both low temperatures and high pressures consists of inorganic $[SbCl_5]^{2-}$ or $[SbCl_6]^{3-}$ distorted polyhedra and ordered organic $[(CH_3)_2NH(CH_2)_2NH_3]^{2+}$ cations. These two oppositely charged moieties are bound together by a system of N(C)−H···Cl hydrogen bonds. The results of this work show that the NNDP crystals exhibit similar behavior at low temperatures and at pressure up to 0.55 GPa, but we find a new phase transition and behavior at higher pressures that is not observed at low temperatures. At 100 and 15 K at room pressure, the structure retains the same space group $P2_1/c$ as at room temperature, with the anionic part of the structure built of isolated $[SbCl_5]^{2-}$ square pyramids. We designate this structure as phase I. The same structure was found at 0.55 GPa (room temperature), but with the Sb···Cl distances between the square pyramids much shorter than at 15 K. Further increase in pressure to 1.00 GPa results in a $P2_1/c \rightarrow P2_1/n$ phase transition accompanied by a doubling of the length of the *a* axis and the formation of $[Sb_2Cl_{10}]^{4-}$ units, each of which consists of one octahedron and one square pyramid that share a common Cl. In this high-pressure $P2_1/n$ phase, which we designate phase II, the interatomic distances significantly decrease on further compression to 4.00 GPa. In particular, the Sb···Cl distances between polyhedra are continuously shortened with increasing pressure to the Sb−Cl bridging bond limit (ca. 3.3 Å).[17−19] As a consequence, zigzag $[\{SbCl_5\}_n]^{2n-}$ chains composed of corner sharing $[SbCl_6]^{3-}$ octahedra are formed at ∼3.1 GPa.

3.1. Phase I. The unit-cell parameters of NNDP crystal decrease almost isotropically and linearly with decreasing temperature from 297 to 15 K. The lengths of *a* and *b* unit-cell parameters decrease by 0.85% and 0.91%, respectively, whereas the *c* parameter decreases by 1.28%. As a result, the unit-cell volume at 15 K is 2.80% less than at room temperature (Table 1).

The structures of phase I at 100 and 15 K exhibit only small changes from the room-temperature structure.[12] The tilt angle between adjacent $[SbCl_5]^{2-}$ pyramids, as defined by the angle between planes containing the four equatorial chlorine atoms,

TABLE 1: Crystal Data and Structure Determination Summary for NNDP

temperature, K	15	100	297	297	297	297	297	297
pressure	0.1 MPa	0.1 MPa	0.1 MPa	0.55 GPa	1.00 GPa	2.00 GPa	3.10 GPa	4.00 GPa
formula	$C_4H_{14}Cl_5N_2Sb$	$C_4H_{14}Cl_5N_2Sb$	$C_4H_{14}Cl_5N_2Sb$	$C_4H_{14}Cl_5N_2Sb$	$C_8H_{28}Cl_{10}N_4Sb_2$	$C_8H_{28}Cl_{10}N_4Sb_2$	$C_8H_{28}Cl_{10}N_4Sb_2$	$C_8H_{28}Cl_{10}N_4Sb_2$
fw, g/mol	389.17	389.17	389.17	389.17	778.34	778.34	778.34	778.34
crystal size, mm^3	0.20 × 0.18 × 0.06	0.12 × 0.09 × 0.03	0.24 × 0.22 × 0.08	0.24 × 0.22 × 0.08	0.24 × 0.22 × 0.08	0.24 × 0.22 × 0.08	0.24 × 0.22 × 0.08	0.24 × 0.22 × 0.08
crystal system	monoclinic	monoclinic	monoclinic	monoclinic	monoclinic	monoclinic	monoclinic	monoclinic
space group, Z	$P2_1/c$, 4	$P2_1/c$, 4	$P2_1/c$, 4	$P2_1/c$, 4	$P2_1/n$, 4	$P2_1/n$, 4	$P2_1/n$, 4	$P2_1/n$, 4
a, Å	12.3542(6)	12.3660(7)	12.484(3)	12.2733(16)	24.6490(12)	24.3137(13)	24.0842(16)	23.969(3)
b, Å	10.1592(5)	10.1778(5)	10.2650(15)	10.1433(6)	10.0612(5)	9.9272(5)	9.7970(6)	9.7129(12)
c, Å	10.1980(5)	10.2219(6)	10.3502(13)	10.0810(5)	10.1210(4)	9.9246(4)	9.7670(4)	9.6721(8)
β, deg	96.839(4)	97.066(4)	97.785(19)	96.782(9)	107.349(7)	107.205(7)	107.171(8)	107.183(16)
V, $Å^3$	1270.83(11)	1276.74(12)	1314.1(4)	1246.22(18)	2395.8(2)	2288.3(2)	2201.8(2)	2151.2(5)
ρ, g/cm^3	2.034	2.025	1.967	2.074	2.158	2.259	2.348	2.403
μ, mm^{-1}	3.180	3.166	3.075	3.243	3.374	3.532	3.671	3.757
θ range, deg	4.01−25.00	4.00−25.00	3.97−25.00	4.02−24.99	2.92−25.00	2.97−25.00	3.01−24.96	3.04−24.99
index ranges	$-14 \le h \le 14$	$-14 \le h \le 14$	$-5 \le h \le 4$	$-5 \le h \le 4$	$-7 \le h \le 15$	$-6 \le h \le 15$	$-7 \le h \le 14$	$-7 \le h \le 14$
	$-12 \le k \le 12$	$-12 \le k \le 12$	$-12 \le k \le 0$	$-12 \le k \le 0$	$0 \le k \le 11$	$0 \le k \le 11$	$0 \le k \le 11$	$0 \le k \le 11$
	$-12 \le l \le 12$	$-12 \le l \le 12$	$0 \le l \le 12$	$0 \le l \le 11$	$-12 \le l \le 0$	$-11 \le l \le 0$	$-11 \le l \le 0$	$-11 \le l \le 0$
reflns collected	16969	17402	7870	7374	14055	13614	13133	12960
completeness, %	97.4	99.6	35.5	35.3	35.4	35.9	36.8	36.8
R_{int}[a]	0.0269	0.0379	0.074	0.034	0.064	0.061	0.056	0.058
data [$I > 2\sigma(I)$]	1968	2180	534	598	897	902	888	857
data/parameters	2173/109	2234/109	822/109	768/109	1485/217	1447/217	1422/217	1398/217
GOF on F^2	1.220	1.191	1.011	0.994	1.087	1.093	1.179	1.113
R_1 [$I > 2\sigma(I)$]	0.0340	0.0226	0.0553	0.0361	0.0566	0.0566	0.0565	0.0597
R_1 (all data)[b]	0.0373	0.0244	0.1183	0.0942	0.1315	0.1583	0.1073	0.1147
wR_2 (all data)[b]	0.0742	0.0355	0.0944	0.0548	0.0878	0.0937	0.1049	0.1310
largest diffraction peak, $e/Å^3$	1.183	0.303	0.420	0.246	0.386	0.614	0.516	0.865
largest diffraction hole, $e/Å^3$	−0.623	−0.361	−0.284	−0.260	−0.348	−0.424	−0.421	−0.508

[a] In the case of the high-pressure data calculated using the Average v2.2 program[33] for reflections with intensities greater than 2σ (I). [b] $R_1 = \sum||F_o| - |F_c||/\sum|F_o|$; $wR_2 = \{\sum[w(F_o^2-F_c^2)^2]/\sum[w(F_o^2)^2]\}^{1/2}$; $w = 1/[\sigma^2(F_o^2) + (aP)^2 + bP]$, where $P = (F_o^2 + 2F_c^2)/3$

TABLE 2: Selected Bond Lengths (Å) and Angles (deg) for NNDP: Low-Temperature Data[a]

atoms/temperature (K)/pressure	15/0.1 MPa	100/0.1 MPa
Sb(1)−Cl(1)	2.3960(10)	2.3912(6)
Sb(1)−Cl(2)	2.4370(11)	2.4336(7)
Sb(1)−Cl(3)	2.9562(11)	2.9603(7)
Sb(1)−Cl(4)	2.5767(11)	2.5682(7)
Sb(1)−Cl(5)	2.6484(11)	2.6491(6)
Sb(1)···Cl(4)^{I}[a]	3.5652(11)	3.5911(7)
Cl(1)−Sb(1)−Cl(2)	91.17(4)	91.20(2)
Cl(1)−Sb(1)−Cl(3)	82.90(3)	82.98(2)
Cl(1)−Sb(1)−Cl(4)	88.07(3)	88.22(2)
Cl(1)−Sb(1)−Cl(5)	84.61(3)	84.63(2)
Cl(2)−Sb(1)−Cl(3)	173.81(3)	173.97(2)
Cl(2)−Sb(1)−Cl(4)	90.44(4)	90.48(2)
Cl(2)−Sb(1)−Cl(5)	86.68(3)	86.68(2)
Cl(3)−Sb(1)−Cl(4)	91.14(3)	90.92(2)
Cl(3)−Sb(1)−Cl(5)	90.98(3)	91.193(19)
Cl(4)−Sb(1)−Cl(5)	172.07(3)	172.25(2)
Cl(1)−Sb(1)···Cl(4)^{I}	160.38(3)	160.36(2)
Cl(2)−Sb(1)···Cl(4)^{I}	91.19(3)	91.32(2)
Cl(3)−Sb(1)···Cl(4)^{I}	93.81(3)	93.639(16)
Cl(4)−Sb(1)···Cl(4)^{I}	111.38(3)	111.228(18)
Cl(5)−Sb(1)···Cl(4)^{I}	76.09(3)	76.076(19)
Sb(1)···Cl(4)^{I}−Sb(1)^{I}	127.24(4)	127.26(2)
N(1)−C(1)	1.489(5)	1.481(3)
C(1)−C(2)	1.517(6)	1.521(4)
N(2)−C(2)	1.478(6)	1.495(3)
N(2)−C(3)	1.528(5)	1.503(3)
N(2)−C(4)	1.500(5)	1.495(3)
N(1)−C(1)−C(2)	110.7(3)	110.2(2)
N(2)−C(2)−C(1)	112.2(3)	111.7(2)
C(2)−N(2)−C(3)	113.3(3)	113.84(19)
C(2)−N(2)−C(4)	111.3(3)	110.3(2)
C(3)−N(2)−C(4)	108.8(3)	109.7(2)
N(1)−C(1)−C(2)−N(2)	172.3(3)	172.8(2)
C(1)−C(2)−N(2)−C(3)	66.0(5)	65.4(3)
C(1)−C(2)−N(2)−C(4)	−171.0(4)	−170.8(2)

[a] Symmetry code: (I) $x, -y + {}^{3}/_{2}, z + {}^{1}/_{2}$.

increases from 53.83(4)° at 297 K to 54.06(2)° at 15 K. The displacement of the Sb^{III} from this plane, a common feature of square pyramidal coordination of Sb^{III},[36] because of the repulsion between the lone electron pair and the bond pairs, increases by 0.018(2) Å on cooling to 15 K. This, together with shortening of the Sb(1)···Cl(4)^{I} distance, suggests the partial movement with decreasing temperature of the lone electron pair from the corner of the $[SbCl_5E]^{2-}$ (E−lone electron pair) octahedron toward the central Sb^{III} atom.

The comparison of the observed Sb−Cl bond lengths and Cl−Sb−Cl angles with the geometry of the isolated $[SbCl_5]^{2-}$ square pyramid not distorted by N−H···Cl hydrogen bonds found in the structure of $[(C_2H_5)_4N]_2[SbCl_5]$[37] further confirms that the distortions of the square pyramids in the low-temperature structures of NNDP are related to the interactions between the oppositely charged organic and inorganic components of the structure. Thus, while the four equatorial Sb−Cl bonds (average 2.602(6) Å) are, to within 2 esd's, identical in the structure of $[(C_2H_5)_4N]_2[SbCl_5]$, the largest differences in bond lengths in NNDP within the basal Sb−Cl bonds are ca. 0.52 Å at both 100 and 15 K (Table 2, Figure 4).

The largest difference in the geometrical parameters of the NNDP structure with decreasing temperature was found for the Sb(1)···Cl(4)^{I} interaction (Table 2). It was shortened by 0.112(3) Å with lowering temperature from 297 to 15 K.[12] The geometry of hydrogen bonds (Table 4) does not change significantly with decreasing temperature, therefore the changes of Sb−Cl and Cl−Sb−Cl parameters are also not significant.

The bond distances and valence angles in organic cations are regular for C(sp^3)−N(sp^3) and C(sp^3)−C(sp^3) bonds. The principal geometrical features are similar to those observed in other compounds containing *N,N*-dimethylethylenediammonium cations,[38,39] but slight differences in conformation reflected in torsion angles are observed[12] (Table 2).

The changes in both the unit-cell and the structural parameters of phase I of NNDP are similar in form, but more pronounced at 0.55 GPa (at room temperature) than at the very lowest temperature, 15 K, at room pressure. As far as the absolute values of the cell constants of NNDP crystal are concerned, cooling to 15 K at ambient pressure is equivalent to applying a pressure of ∼0.4 GPa at room temperature (Table 1). This is similar to the results of other low-temperature, high-pressure studies of molecular materials undergoing no structural phase transitions.[40,41] Pressure, like temperature, has little effect upon either the bond lengths and angles of the organic part of the structure or the hydrogen bond geometries (Tables 2, 3, and 4). But a significant difference is found at pressure in the case of the interpolyhedral Sb(1)···Cl(4)^{I} distance, which decreases by 0.173(9) Å. The deviations of the Sb−Cl bond lengths from the values of 2.346(4) for axial and 2.602(6) Å for equatorial chlorine atoms found in the reference-isolated square pyramid[37] are smaller at 297 K and 0.55 GPa than at 15 K and 0.1 MPa (Tables 2 and 3).

3.2. Phase Transition. The pressure dependence of the normalized unit-cell parameters and unit-cell volume between room pressure and 4.00 GPa is shown in Figure 5. Clear discontinuous changes in a, c, and β parameters, as well as in the unit-cell volume V, are observed between 0.55 and 1.00 GPa. The values of the a and c parameters as well as the monoclinic β angle increase from 0.55 and 1.00 GPa, while the unit-cell parameter b decreases. Calculation of the resulting strain tensor shows that the direction of maximum expansion is approximately parallel to $[10\bar{1}]$, while the perpendicular plane exhibits compression. Overall, this leads to a decrease of the unit-cell volume by 3.88%. The transition was found to be completely reversible: the NNDP crystal returned to the $P2_1/c$ low-temperature/low-pressure phase I after the DAC was unloaded back to the ambient pressure.

The diffraction data show that the pressure-induced phase transition in NNDP is characterized by a change in the space group from $P2_1/c$ to $P2_1/n$, together with a doubling of the unit-cell parameter a and thus the number of atoms in the unit cell (Figure 6). At the transition, the coordination of ${}^{1}/_{2}$ of the Sb atoms is increased from 5 to 6, with the resulting $[SbCl_5]^{2-}$ pyramids and $[SbCl_6]^{3-}$ octahedra alternating along [001]. This alternation destroys the c-glide symmetry element of phase I, and the offset of the octahedra in next-neighbor chains along [100] results in the doubling of length of the a-axis. This, and the associated loss of ${}^{1}/_{2}$ of the centers of symmetry and ${}^{1}/_{2}$ of the diad axes, results in the change in space group symmetry from $P2_1/c$ to $P2_1/n$ (Figure 6).

The driving force for the transition appears to be an instability in the interactions between the Sb atoms and the Cl(4) atoms of neighboring $[SbCl_5]^{2-}$ pyramids within phase I, shown as dashed lines in Figure 6a. This contact shows the greatest decrease of Sb−Cl distances in phase I from ambient pressure to 0.55 GPa, and extrapolation of this trend would result in an interpyramidal Sb(1)···Cl(4)^{I} distance of about 3.4 Å at 1.00 GPa. Instead, this single nonbonding distance splits into two symmetry-independent distances of Sb(11)−Cl(24) = 3.302(5) Å and Sb(21)···Cl(14)^{II} = 3.558(5) Å (Table 3, Figure 7). The shorter distance is similar to the bridging Sb−Cl bond distances found in other chloroantimonates(III), whereas the longer one is considered to be a nonbonding interaction.[17,19,38,42]

TABLE 3: Selected Bond Lengths (Å) and Angles (deg) for NNDP: High-Pressure Data[a]

atoms/temperature (K)/pressure	297/0.1MPa	297/0.55GPa	297 K/1.00 GPa		297 K/2.00 GPa		297 K/3.10 GPa		297 K/4.00 GPa	
Sb(1)−Cl(1)|Sb(11)/(21)−Cl(11)/(21)	2.369(5)	2.381(4)	2.396(6)	/2.406(7)	2.385(6)	/2.386(7)	2.386(7)	/2.381(7)	2.394(7)	/2.375(8)
Sb(1)−Cl(2)|Sb(11)/(21)−Cl(12)/(22)	2.421(8)	2.423(5)	2.415(8)	/2.457(8)	2.405(8)	/2.448(7)	2.389(8)	/2.454(8)	2.395(9)	/2.452(9)
Sb(1)−Cl(3)|Sb(11)/(21)−Cl(13)/(23)	2.947(6)	2.940(4)	2.964(8)	/2.890(8)	2.948(8)	/2.846(8)	2.950(8)	/2.827(8)	2.932(9)	/2.849(9)
Sb(1)−Cl(4)|Sb(11)/(21)−Cl(14)/(24)	2.550(5)	2.585(3)	2.550(6)	/2.537(5)	2.564(6)	/2.533(5)	2.560(6)	/2.544(6)	2.573(7)	/2.541(6)
Sb(1)−Cl(5)|Sb(11)/(21)−Cl(15)/(25)	2.678(6)	2.624(3)	2.657(6)	/2.653(6)	2.615(6)	/2.632(5)	2.595(6)	/2.601(6)	2.573(7)	/2.585(6)
Sb(1)···Cl(4)^{I}|Sb(11)/(21)···Cl(24)/(14)^{II}	3.682(6)	3.509(3)	3.302(5)	/3.558(5)	3.191(5)	/3.416(5)	3.124(5)	/3.297(5)	3.080(6)	/3.238(6)
Cl(1)−Sb(1)−Cl(2)|Cl(11)/(21)−Sb(11)/(21)−Cl(12)/(22)	90.5(2)	90.56(15)	92.5(2)	/89.2(2)	91.7(2)	/88.1(2)	91.2(3)	/87.7(3)	91.2(3)	/88.0(3)
Cl(1)−Sb(1)−Cl(3)|Cl(11)/(21)−Sb(11)/(21)−Cl(13)/(23)	83.98(19)	83.03(11)	84.9(2)	/81.1(2)	85.2(2)	/80.9(2)	84.9(2)	/80.5(2)	84.1(2)	/79.9(3)
Cl(1)−Sb(1)−Cl(4)|Cl(11)/(21)−Sb(11)/(21)−Cl(14)/(24)	88.2(2)	87.93(12)	87.6(2)	/87.7(2)	87.1(2)	/86.6(2)	86.6(2)	/86.5(2)	86.6(2)	/86.4(2)
Cl(1)−Sb(1)−Cl(5)|Cl(11)/(21)−Sb(11)/(21)−Cl(15)/(25)	84.74(17)	84.95(11)	84.31(19)	/83.63(18)	84.52(18)	/83.45(18)	84.3(2)	/83.5(2)	84.4(2)	/83.0(2)
Cl(2)−Sb(1)−Cl(3)|Cl(12)/(22)−Sb(11)/(21)−Cl(13)/(23)	174.3(2)	173.19(14)	177.3(2)	/169.77(19)	176.7(2)	/168.45(19)	175.6(3)	/167.6(2)	174.9(3)	/167.2(2)
Cl(2)−Sb(1)−Cl(4)|Cl(12)/(22)−Sb(11)/(21)−Cl(14)/(24)	91.2(2)	90.30(13)	92.6(2)	/89.5(2)	91.8(2)	/89.8(2)	92.0(2)	/88.8(2)	91.2(3)	/88.2(2)
Cl(2)−Sb(1)−Cl(5)|Cl(12)/(22)−Sb(11)/(21)−Cl(15)/(25)	86.9(2)	86.22(13)	88.2(2)	/88.4(2)	87.5(2)	/87.6(2)	86.6(3)	/87.0(2)	86.2(3)	/86.6(2)
Cl(3)−Sb(1)−Cl(4)|Cl(13)/(23)−Sb(11)/(21)−Cl(14)/(24)	90.12(19)	91.76(11)	88.1(2)	/86.8(2)	89.3(2)	/86.1(2)	89.8(2)	/86.7(2)	90.6(2)	/87.2(3)
Cl(3)−Sb(1)−Cl(5)|Cl(13)/(23)−Sb(11)/(21)−Cl(15)/(25)	91.16(18)	90.91(11)	90.7(2)	/93.8(2)	91.1(2)	/94.5(2)	91.0(2)	/95.4(2)	91.3(3)	/95.7(3)
Cl(4)−Sb(1)−Cl(5)|Cl(14)/(24)−Sb(11)/(21)−Cl(15)/(25)	172.67(16)	172.04(8)	171.9(2)	/171.12(18)	171.60(17)	/169.82(18)	170.74(18)	/169.29(17)	170.55(18)	/168.41(17)
Cl(1)−Sb(1)···Cl(4)^{I}|Cl(11)/(21)−Sb(11)/(21)−Cl(24)/(14)^{II}	160.5(2)	161.09(12)	159.2(2)	/152.2(2)	158.5(2)	/153.2(2)	158.3(2)	/153.4(2)	157.9(2)	/153.7(2)
Cl(2)−Sb(1)···Cl(4)^{I}|Cl(12)/(22)−Sb(11)/(21)−Cl(24)/(14)^{II}	91.95(19)	90.99(11)	87.61(18)	/95.78(19)	87.15(17)	/95.49(19)	85.83(19)	/94.9(2)	85.3(2)	/93.4(2)
Cl(3)−Sb(1)···Cl(4)^{I}|Cl(13)/(23)−Sb(11)/(21)−Cl(24)/(14)^{II}	92.78(13)	94.33(8)	94.53(15)	/94.34(15)	95.32(16)	/95.91(15)	97.07(17)	/97.37(17)	98.25(18)	/99.29(19)
Cl(4)−Sb(1)···Cl(4)^{I}|Cl(14)/(24)−Sb(11)/(21)−Cl(24)/(14)^{II}	111.1(2)	110.91(14)	113.14(19)	/119.56(19)	114.33(19)	/119.90(19)	115.0(2)	/120.0(2)	115.2(3)	/119.9(3)
Cl(5)−Sb(1)···Cl(4)^{I}|Cl(15)/(25)−Sb(11)/(21)−Cl(24)/(14)^{II}	76.06(16)	76.35(10)	74.92(18)	/69.26(17)	74.00(17)	/70.18(17)	74.1(2)	/70.24(19)	73.7(2)	/70.8(2)
Sb(1)···Cl(4)^{I}−Sb(1)^{I}|	128.0(3)	126.20(18)	133.2(3)	/128.3(3)	133.2(3)	/127.0(3)	131.3(4)	/126.3(3)	130.3(4)	/124.8(4)
|Sb(11)/(11)−Cl(24)/(14)−Sb(21)/(21)^{III}										
N(1)−C(1)|N(11)/(21)−C(11)/(21)	1.47(3)	1.50(2)	1.51(4)	/1.50(3)	1.46(4)	/1.41(3)	1.52(4)	/1.36(4)	1.46(4)	/1.44(4)
C(1)−C(2)|C(11)/(21)−C(12)/(22)	1.38(3)	1.48(2)	1.41(3)	/1.61(4)	1.52(4)	/1.60(4)	1.62(4)	/1.60(4)	1.59(4)	/1.67(5)
N(2)−C(2)|N(12)/(22)−C(12)/(22)	1.54(3)	1.445(17)	1.47(4)	/1.36(3)	1.43(3)	/1.37(3)	1.40(3)	/1.38(3)	1.50(4)	/1.27(3)
N(2)−C(3)|N(12)/(22)−C(13)/(23)	1.45(2)	1.525(17)	1.48(3)	/1.48(3)	1.48(3)	/1.49(3)	1.49(3)	/1.49(3)	1.40(3)	/1.50(3)
N(2)−C(4)|N(12)/(22)−C(14)/(24)	1.49(3)	1.51(2)	1.48(2)	/1.44(2)	1.49(2)	/1.47(3)	1.48(2)	/1.46(3)	1.47(3)	/1.50(4)
N(1)−C(1)−C(2)|N(11)/(21)−C(11)/(21)−C(12)/(22)	106.8(14)	110.9(8)	111.1(15)	/116.6(12)	112.0(14)	/114.5(12)	114.4(13)	/112.5(14)	111.4(15)	/117.1(14)
N(2)−C(2)−C(1)|N(12)/(22)−C(12)/(22)−C(11)/(21)	111.1(13)	108.9(7)	114.3(15)	/114.0(13)	113.7(14)	/116.2(13)	112.0(13)	/113.2(14)	114.0(13)	/112.7(16)
C(2)−N(2)−C(3)|C(12)/(22)−N(12)/(22)−C(13)/(23)	110.9(12)	115.3(7)	115.8(14)	/111.9(13)	109.7(14)	/114.3(13)	108.1(14)	/112.1(13)	110.9(15)	/109.4(15)
C(2)−N(2)−C(4)|C(12)/(22)−N(12)/(22)−C(14)/(24)	113.0(13)	110.3(8)	112.7(14)	/107.1(13)	110.8(13)	/111.9(12)	107.0(14)	/109.0(14)	108.4(14)	/107.6(15)
C(3)−N(2)−C(4)|C(13)/(23)−N(12)/(22)−C(14)/(24)	110(2)	105.6(14)	109(2)	/112(2)	111(2)	/110(2)	111(3)	/108(3)	114(3)	/104(3)
N(1)−C(1)−C(2)−N(2)|	173.5(16)	171.0(11)	174(2)	−167.7(19)	170(2)	−172(2)	166(2)	−172(2)	173(2)	−164(2)
|N(11)/(21)−C(11)/(21)−C(12)/(22)−N(12)/(22)										
C(1)−C(2)−N(2)−C(3)|	60(2)	67.6(15)	65(3)	−68(3)	74(3)	−63(3)	78(3)	−70(3)	71(3)	−75(3)
|C(11)/(21)−C(12)/(22)−N(12)/(22)−C(13)/(23)										
C(1)−C(2)−N(2)−C(4)|	−176(2)	−172.9(12)	−168.8(19)	169.1(18)	−163.6(19)	170.7(19)	−162.7(19)	170(2)	−162(2)	172(2)
|C(11)/(21)−C(12)/(22)−N(12)/(22)−C(14)/(24)										

[a] Symmetry codes: (I) x, $-y + {}^{3}/_{2}$, $z + {}^{1}/_{2}$; (II) x, y, $z + 1$; (III) x, y, $z - 1$

TABLE 4: Strongest N−H···Cl Hydrogen Bond Geometries (Å, deg) at Selected Temperature and Pressure Points in Both Phases of NNDP[a]

D−H···A	D−H	H···A	D···A	D−H···A
	15 K/0.1 MPa			
N(1)−H(1)···Cl(3)^{I}	0.89	2.32	3.172(4)	160.2
N(1)−H(2)···Cl(3)^{II}	0.89	2.32	3.198(4)	167.2
N(1)−H(3)···Cl(5)^{III}	0.89	2.34	3.223(4)	170.1
N(2)−H(8)···Cl(3)	0.91	2.46	3.200(4)	138.0
	297 K/0.1 MPa			
N(1)−H(1)···Cl(3)^{I}	0.89	2.39	3.255(16)	162.9
N(1)−H(2)···Cl(3)^{II}	0.89	2.40	3.268(15)	165.9
N(1)−H(3)···Cl(5)^{III}	0.89	2.32	3.201(14)	169.2
N(2)−H(8)···Cl(3)	0.91	2.48	3.22(2)	138.9
	297 K/0.55 GPa			
N(1)−H(1)···Cl(3)^{I}	0.89	2.31	3.166(11)	162.4
N(1)−H(2)···Cl(3)^{II}	0.89	2.32	3.203(10)	170.6
N(1)−H(3)···Cl(5)^{III}	0.89	2.36	3.215(10)	161.9
N(2)−H(8)···Cl(3)	0.91	2.49	3.234(13)	138.9
	297 K/1.00 GPa			
N(11)−H(111)···Cl(13)^{IV}	0.89	2.23	3.086(17)	160.1
N(11)−H(112)···Cl(23)^{V}	0.89	2.31	3.175(19)	164.0
N(11)−H(113)···Cl(15)^{III}	0.89	2.26	3.140(18)	167.9
N(12)−H(118)···Cl(13)	0.91	2.54	3.22(2)	132.2
N(21)−H(211)···Cl(23)^{V}	0.89	2.31	3.168(17)	160.7
N(21)−H(212)···Cl(13)^{V}	0.89	2.25	3.129(18)	171.2
N(21)−H(213)···Cl(25)	0.89	2.40	3.245(18)	159.2
N(22)−H(218)···Cl(23)^{III}	0.91	2.48	3.22(2)	138.8
	297 K/4.00 GPa			
N(11)−H(111)···Cl(13)^{IV}	0.89	2.13	2.96(2)	154.8
N(11)−H(112)···Cl(23)^{V}	0.89	2.22	3.10(2)	174.3
N(11)−H(113)···Cl(11)^{III}	0.89	2.83	3.29(2)	113.1
N(11)−H(113)···Cl(15)^{III}	0.89	2.30	3.14(2)	158.1
N(12)−H(118)···Cl(13)	0.91	2.52	3.16(3)	128.3
N(12)−H(118)···Cl(25)^{VI}	0.91	2.63	3.30(2)	130.5
N(21)−H(211)···Cl(23)^{V}	0.89	2.26	3.12(2)	163.1
N(21)−H(212)···Cl(13)^{V}	0.89	2.18	3.07(2)	173.7
N(21)−H(213)···Cl(21)	0.89	2.73	3.193(18)	113.8
N(21)−H(213)···Cl(25)	0.89	2.29	3.14(2)	158.3
N(22)−H(218)···Cl(23)^{III}	0.91	2.38	3.10(3)	136.6
N(22)−H(218)···Cl(24)^{III}	0.91	2.73	3.267(15)	118.9

[a] Symmetry codes: (I) $-x+1, y-1/2, -z+1/2$; (II) $-x+1, -y+1, -z+1$; (III) $x, y-1, z$; (IV) $-x+1/2, y-1/2, -z+1/2$; (V) $-x+1/2, y-1/2, -z+3/2$; (VI) $x, y, z-1$.

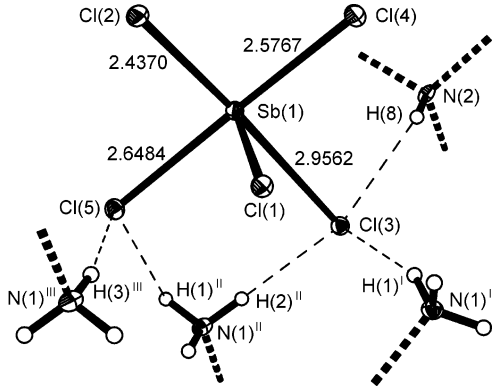

Figure 4. N−H···Cl hydrogen bonds (thin dashed lines), which cause the distortion of $[SbCl_5]^{2-}$ units in the structure of NNDP at 15 K and 0.1 MPa. Displacement ellipsoids are drawn at 50% probability level. Symmetry codes: (I) $-x+1, y+1/2, -z+1/2$; (II) $-x+1, -y+1, -z+1$; (III) $x, y+1, z$.

As a result, the isolated $[SbCl_5]^{2-}$ square pyramids of phase I are transformed into $[Sb_2Cl_{10}]^{4-}$ units in phase II (Figure 6b). This discontinuity in the compression of the interpolyhedral distances in NNDP crystal suggests that the ca. 3.3 Å distance between Sb and Cl atoms should be considered as a limit for the bridging Sb−Cl bonds.[12]

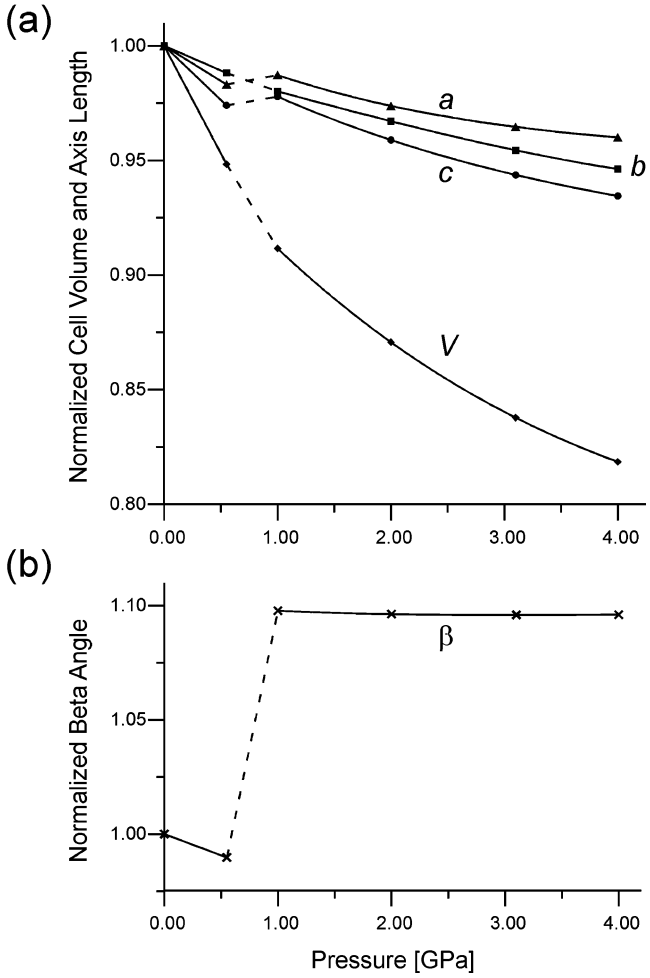

Figure 5. Pressure dependence of normalized cell volume V and axis length a, b, c (a) as well as normalized monoclinic β angle (b) of the NNDP crystal. For the 1.00−4.00 GPa range, the $a/2$ and $V/2$ values of the space group $P2_1/n$ were used. The variations of the unit-cell parameters and volume were fitted to linear and polynomial functions in two regions: 0.00−0.55 and 1.00−4.00 GPa, respectively.

The phase transition in NNDP is an example of a pressure-driven conversion of the Sb^{III} electron configuration from a lone electron pair occupying the corner of the $[SbCl_5E]^{2-}$ octahedron to a lone electron pair which, formally, occupies an s orbital. However, it is clear from the residual distortion of the coordination around the Sb^{III} that the lone electron pair retains stereochemical activity and is not spherically distributed around the central antimony(III) atom. A similar pressure-induced phase transition involving the conversion of the electron configuration of Ge^{II} was found in $CsGeBr_3$, but in contrast to the phase transition occurring in NNDP, in this case, the lone electron pair shows the pure s-orbital character, reflected in the nondistorted geometry of $[GeBr_6]^{4-}$ octahedron.[43]

3.3. Phase II. The a, b, and c unit-cell parameters decrease similarly by 2.76, 3.46, and 4.44% respectively from 1.00 to 4.00 GPa. This leads to a change in the unit-cell volume of 10.21% over the 3 GPa pressure range. Further pressure increase was precluded by the development of significant nonhydrostatic stresses in the pressure medium. The data are not sufficient to unambiguously determine the equation of state (EoS) parameters for phase II, but it is clear (Figure 5) that it is stiffer than phase I, presumably as a result of the formation of the new Sb−Cl bonds between polyhedra along the [001] direction that results in a significant stiffening of this direction in phase II. A fit of a Murnahan EoS[44] with $K' = dK/dP$ fixed at 4 yields a room

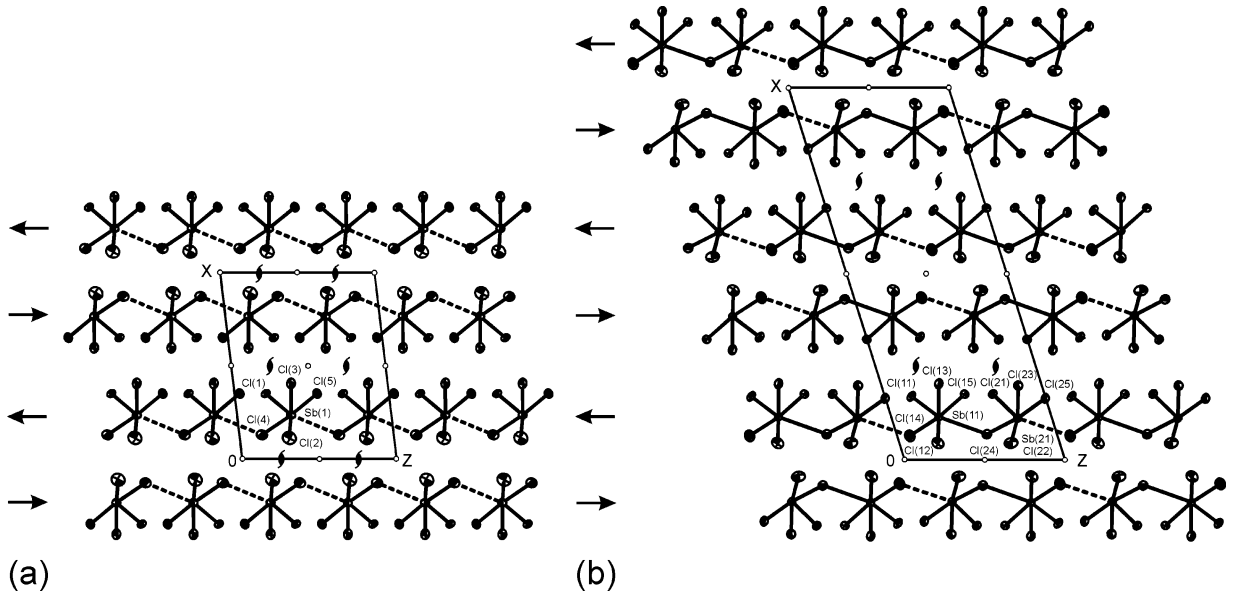

Figure 6. Anionic substructures of NNDP crystal in the low-temperature/low-pressure $P2_1/c$ at 297 K and 0.55 GPa (a) and high-pressure $P2_1/n$ at 297 K and 1.00 GPa (b) phases, along their *b* axes. The arrows denote the orientation of the apical Sb−Cl bonds in the $[SbCl_5]^{2-}$ pyramids in each chain. The positions of the screw diad axes and the inversion centers are also indicated.

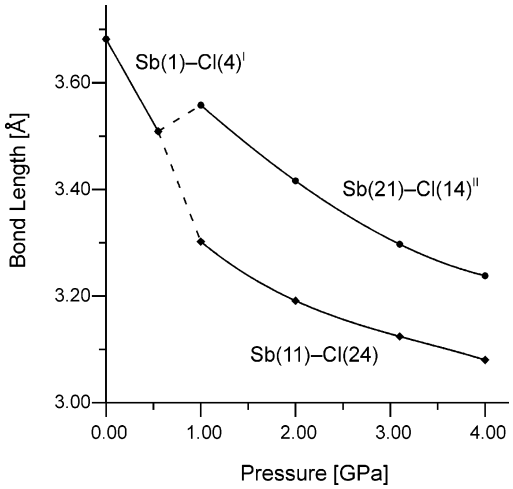

Figure 7. Pressure dependence of the bridging antimony···chlorine distances in both phases of NNDP. Symmetry codes: (I) $x, -y + 3/2, z + 1/2$; (II) $x, y, z + 1$.

pressure bulk modulus, K_0, for phase II of 18.5(1.5) GPa which, given the curvature of the $V-P$ plot (Figure 5) is probably an overestimate of the true value. Simultaneous refinement of K_0 and K' yields values of $K_0 = 8(3)$ GPa and $K' = 8.7(1.5)$.

There are two symmetry-independent Sb(11) and Sb(21) inorganic polyhedra as well as two symmetry-independent organic cations in the high-pressure phase II of NNDP. At 1.00 GPa the Sb(11) has octahedral coordination, while the Sb(21) remains five-coordinated by Cl, and these polyhedra are linked through the Cl(24) to form $[Sb_2Cl_{10}]^{4-}$ isolated units, with a nonbonded Sb(21)···Cl(14)^{II} distance between adjacent units. As pressure is increased, the Sb(21)···Cl(14)^{II} distance rapidly decreases from 3.558(5) Å at 1.00 GPa to less than 3.3 Å at 3.10 GPa, at which point Sb(21)···Cl(14)^{II} can be considered bonded (Figure 7). This rapid decrease in Sb−Cl distances subparallel to [001] is responsible for this being the most compressible direction in the structure. Pressure thus appears to continuously convert the $[Sb_2Cl_{10}]^{4-}$ isolated units to $[\{SbCl_5\}_n]^{2n-}$ chains of corner-sharing $[SbCl_6]^{3-}$ octahedra. Despite this conversion of both Sb atoms to octahedral coordination, they remain symmetrically distinct with different Sb−Cl bond geometries (Table 3). The existence of two chemically equivalent but symmetrically distinct $[SbCl_6]^{3-}$ groups within the structure is unusual; one might expect instead the reversion of the structure to the $P2_1/c$ symmetry of phase I, but with a single symmetrically distinct Sb site in octahedral coordination by Cl. However, the observation of significant numbers of *hkl* reflections with h = odd in the diffraction patterns collected at 4.00 GPa confirms that the *a*-axis remains doubled, eliminating the possibility of reversion to the unit cell of phase I. Similarly, the observation of l = odd reflections eliminates the possibility of the *c*-unit-cell parameter being halved, and the deviation of the unit-cell parameters from higher-metric symmetry eliminates orthorhombic or higher symmetries.

Both Sb atoms occupy general positions in the structure of phase II, so their coordination geometry is therefore not constrained by symmetry. All of the Sb−Cl bonds within a polyhedron can be of different lengths, and the distortion of the Sb−Cl polyhedra is free to evolve in any way. However, the lengths of both the equatorial bonds and the apical bond inherited from phase I change very little with pressure, and the most significant changes are the large decrease of the sixth Sb−Cl bond in both octahedra. However, although the longer Sb(21)−Cl(14)^{II} distance, which is nonbonded at 1.00 GPa, decreases faster than the bonded Sb(11)−Cl(24) distance, they do not become equal by 4.00 GPa (Figure 7). It is this difference that maintains the distinction between the Sb(11) and Sb(21) sites and the symmetry as $P2_1/n$.

The tilt angle between adjacent polyhedra (as defined by the planes of the four equatorial ligands) remains almost the same (average 53.9(2)°), within 3 esd's, up to 4.00 GPa. There is, however, a small increase in the angular distortion of the polyhedra measured by the parameter $\sigma^2 = 1/a \sum_{i=1}^{a+1} (\alpha_i - 90°)^2$ (a = 7 or 11) calculated from the α_i, the individual cis Cl−Sb−Cl bond angles.[45] This is, in part, due to an increasing displacement toward the long sixth Sb−Cl bond with pressure of both the Sb atoms from the planes defined by their four equatorial Cl ligands, from 0.121(3) and 0.213(4) Å at 1.00 GPa to 0.157(4) and 0.263(4) Å at 4.00 GPa. This again indicates that, although the change to octahedral coordination indicates

that the lone electron pair was moved from the corner of the $[SbCl_5E]^{2-}$ octahedron toward the nucleus of the central Sb(11) and Sb(21) atoms and, formally, occupies the s orbital, it is still stereochemically active and oriented toward the longest Sb−Cl bond.[9,46]

Only slight modifications of the organic cation geometries are observed when pressure is applied (Table 3). Increasing pressure leads, in general, to an increase in the strength and the number of the hydrogen bonds (Table 4).

4. Summary and Concluding Remarks

This is, to the best of our knowledge, the first study of an organic−inorganic hybrid antimony(III) structure by single-crystal diffraction at high pressures. The use of a CCD camera with a diamond-anvil cell for single-crystal diffraction requires the use of modified data collection and data reduction procedures, e.g., ref 35, but has, in this study, been shown to result in refinement parameters and a refined structure that is comparable in precision to those obtained under ambient conditions or low temperatures in air. In particular, we found it was possible to refine the positions of the C and N atoms forming the backbone of the organic cations in the high-pressure structures even though the diffraction intensities are dominated by scattering from the much heavier Sb and Cl atoms of the inorganic component of the structure. This indicates that we will be able to detect the expected pressure-induced ordering of organic cations in related structures in which they are dynamically disordered at room conditions.

Our study of NNPD also illustrates that, in these hybrid materials, the effects of quite modest pressures far exceed the structural changes that occur on cooling to low temperatures. Thus, we found that the structural changes that occurred upon compression to 0.55 GPa were similar to, but exceeded in magnitude, the changes induced by cooling the crystal from room temperature to 15 K at ambient pressure. Because the organic cations in NNPD are already ordered at room conditions, this similarity in behavior at high pressure and low temperature indicates that the structural changes in both cases are driven by reduction in the unit-cell volume and not, in the case of low temperature, directly by a reduction in thermal energy available to the system.

The small changes within phase I upon both cooling and upon pressurization appear to be the result of a slight shift of the lone electron pair from the corner of the $[SbCl_5E]^{2-}$ octahedron toward the central Sb^{III} atom. This appears confirmed by the structural changes that occur at the subsequent high-pressure phase transition to phase II. In phase II $^1/_2$ of the Sb atoms become 6-coordinated by Cl, indicating that the lone electron pair on these atoms have become, formally, localized in a spherical s-orbital. The fact that every other Sb atom in the structure initially retains 5-fold coordination by Cl points to the existence of either long-range electronic interactions along the chains or to simple steric considerations preventing the further shortening of the chains to allow 6 coordination for all Sb atoms. Whichever is the cause, further pressure increase leads to shortening of the longer Sb···Cl contacts until distorted octahedral coordination for all Sb atoms is attained at ∼3.1 GPa. Even at the highest pressures achieved in these experiments, with a volume compression of 18.15% from room pressure, the Sb atoms remain displaced from the centers of their coordination octahedra, suggesting that the lone electron pair retains some stereochemical activity.

Phase II of NNDP therefore presents an interesting hybrid of behavior in that one of these coordination changes is achieved through a discontinuous phase transition, while the other is achieved continuously upon further compression. Further, the large changes in the structure of the inorganic component of the structure, in the absence of changes in the state of dynamic order of the organic cations, show that the structural changes and phase transitions in this general class of organic−inorganic hybrids are not always dominated or driven by changes in the ordering of the dynamic motions of the cations, but can arise from intrinsic processes in the inorganic component alone.

Acknowledgment. This material is based upon work supported by the North Atlantic Treaty Organization under a grant awarded in 2004 (DGE−0410297). Virginia Tech provided funds for the purchase of the Oxford Diffraction Xcalibur-1 diffractometer. We acknowledge financial support from the National Science Foundation (CHE-0131128) for the purchase of the Oxford Diffraction Xcalibur-2 diffractometer. Ruby pressure measurements were conducted with the Raman system in the Vibrational Spectroscopy Laboratory in the Department of Geosciences at Virginia Tech. We are grateful to Dr. C. Slebodnick (Department of Chemistry, Virginia Tech), Dr. N. Vogelaar (Department of Biological Sciences, Virginia Tech) and Mr. D. Warner (Oxford Diffraction Ltd) for valuable discussions and help during the low-temperature (15 K) X-ray experiment. We thank Prof. B. Hanson (Department of Chemistry, Virginia Tech) for providing the starting materials and opportunity to prepare crystals in his laboratory.

Supporting Information Available: Crystallographic data in CIF format. This material is available free of charge via the Internet at http://pubs.acs.org.

References and Notes

(1) Fischer, G. A.; Norman, N. C. *Adv. Inorg. Chem.* **1994**, *41*, 233−271.
(2) Sobczyk, L.; Jakubas, R.; Zaleski, J. *Pol. J. Chem.* **1997**, *71*, 265−300.
(3) Bujak, M.; Zaleski, J. *J. Solid State Chem.* **2004**, *177*, 3202−3211.
(4) Alcock, N. W. *Adv. Inorg. Radiochem.* **1972**, *15*, 1−58.
(5) Landrum, G. A.; Hoffmann, R. *Angew. Chem., Int. Ed.* **1998**, *37*, 1887−1890.
(6) Starbuck, J.; Norman, N. C.; Orpen, A. G. *New J. Chem.* **1999**, *23*, 969−972.
(7) Akiba, K.-y., Ed. *Chemistry of Hypervalent Compounds*; Wiley-VCH: New York, 1999.
(8) Gillespie, R. J.; Nyholm, R. S. *Q. Rev. Chem. Soc.* **1957**, *11*, 339−380.
(9) Gillespie, R. J.; Robinson, E. A. *Chem. Soc. Rev.* **2005**, *34*, 396−407.
(10) Bujak, M.; Osadczuk, P.; Zaleski, J. *Acta Crystallogr., Sect C* **2001**, *57*, 388−391.
(11) Bujak, M.; Zaleski, J. *Z. Naturforsch., B: Chem. Sci.* **2002**, *57*, 157−164.
(12) Bujak, M.; Zaleski, J. *Z. Naturforsch., B: Chem. Sci.* **2001**, *56*, 521−525.
(13) Olivier-Fourcade, J.; lbanez, A.; Jumas, J. C.; Maurin, M.; Lefebvre, I.; Lippens, P.; Lannoo, M.; Allan, G. *J. Solid State Chem.* **1990**, *87*, 366−377.
(14) Wang, X.; Liebau, F. *Acta Crystallogr., Sect. B* **1996**, *52*, 7−15.
(15) Galy, J.; Enjalbert, R. *J. Solid State Chem.* **1982**, *44*, 1−23.
(16) Zaleski, J.; Pietraszko, A. *Acta Crystallogr., Sect. B* **1996**, *52*, 287−295.
(17) Bujak, M.; Zaleski, J. *Cryst. Eng.* **2001**, *4*, 241−252.
(18) Bujak, M.; Angel, R. J. *J. Solid State Chem.* **2005**, *178*, 2237−2246.
(19) Bujak, M.; Zaleski, J. *Acta Crystallogr., Sect. C* **1998**, *54*, 1773−1777.
(20) Bujak, M.; Angel, R. J. to be published.
(21) *CrysAlis CCD, Data Collection GUI for CCD and CrysAlis RED CCD Data Reduction GUI*, versions 1.171.24 beta (release 23.09.2004); Oxford Diffraction: Wrocław, Poland, 2004.
(22) Allan, D. R.; Miletich, R.; Angel, R. J. *Rev. Sci. Instrum.* **1996**, *67*, 840−844.

(23) Miletich, R.; Allan, D. R.; Kuhs, W. *Rev. Mineral. Geochem.* **2000**, *41*, 445−519.
(24) Angel, R. J.; Bujak, M.; Zhao, J.; Jacobsen, S. D. *Rev. Sci. Instrum.* submitted.
(25) Piermarini, G. J.; Block, S.; Barnett, J. D.; Forman, R. A. *J. Appl. Phys.* **1975**, *46*, 2774−2780.
(26) Dera, P.; Katrusiak, A. *J. Appl. Crystallogr.* **1999**, *32*, 510−515.
(27) Angel, R. J. *J. Appl. Crystallogr.* **2003**, *36*, 295−300.
(28) Angel, R. J.; Downs, R. T.; Finger, L. W. *Rev. Mineral. Geochem.* **2000**, *41* 559−596.
(29) King, H. E.; Finger, L. W. *J. Appl. Crystallogr.* **1979**, *12*, 374−378.
(30) Ralph, R. L.; Finger, L. W. *J. Appl. Crystallogr.* **1982**, *15*, 537−539.
(31) Angel, R. J. *J. Appl. Crystallogr.* **2004**, *37*, 486−492.
(32) Burham, C. W. *Am. Mineral.* **1996**, *51*, 159−167.
(33) Angel, R. J. *Average v2.2, A Program to Merge Single-Crystal Diffraction Intensity Data, with Rejection of Outliers*; Crystallography Laboratory, Department of Geosciences, Virginia Tech: Blacksburg, VA, 2003; www.crystal.vt.edu.
(34) Sheldrick, G. M. *SHELXTL NT*, version 6.12; Bruker Analytical X-ray Systems, Inc.: Madison, WI, 2001.
(35) Angel, R. J. In *Advances in High-Pressure Techniques for Geophysical Applications*; Chen, J., Wang, Y., Duffy, T. S., Shen, G., Dobrzhinetskaya, L. P, Eds.; Elsevier Science: Amsterdam, 2005; pp 371−396.
(36) Kruss, B.; Ziegler, L. Z. *Anorg. Allg. Chem.* **1972**, *388*, 158−164.
(37) Zaleski, J.; Pietraszko, A. *J. Phys. Chem. Solids* **1995**, *56*, 883−890.
(38) Bujak, M.; Zaleski, J. *Main Group Met. Chem.* **2002**, *25*, 571−577.
(39) Doran, M. B.; Norquist, A. J.; O'Hare, D. *Inorg. Chem.* **2003**, *42*, 6989−6995.
(40) Guionneau, P.; Gaultier, J.; Chasseau, D.; Bravic, G.; Barrans, Y.; Ducasse, L.; Kanazawa, D.; Day, P.; Kurmoo, M. *J. Phys. Fr.* **1996**, *6*, 1581−1595.
(41) Guionneau, P.; Brigouleix, C.; Barrans, Y.; Goeta, A. E.; Létard, J. F.; Howard, J. A. K.; Gaultier, J.; Chasseau, D. *C. R. Acad. Sci., Ser. IIc: Chim.* **2001**, *4*, 161−171.
(42) Bujak, M.; Zaleski, J. *Acta Crystallogr., Sect. C* **1999**, *55*, 1775−1778.
(43) Schwarz, U.; Hillebrecht, H.; Kaupp, M.; Syassen, K.; von Schnering, H.-G. *J. Solid State Chem.* **1995**, *118*, 20−27.
(44) Murnaghan, F. D. *Am. J. Math.* **1937**, *49*, 235−260.
(45) Robinson, K.; Gibbs, G. V.; Ribbe, P. H. *Science* **1971**, *172*, 567−570.
(46) Wheeler, R. A.; Kumar, P. N. V. P. *J. Am. Chem. Soc.* **1992**, *114*, 4776−4784.